

Article

Curing Agent for High-Concentration Unclassified Tailings Stockpiling: A Case Study of Tailings from a Gold Mine

Weixiang Wang^{1,2}, Kun Li^{1,2,*}, Lijie Guo^{1,2,*}, Sha Wang^{1,2}, Yifan Chu^{1,2} and Yao Lu^{1,2}

¹ BGRIMM Technology Group, Beijing 102628, China; wangweixiang@bgrimm.com (W.W.); wangsha@bgrimm.com (S.W.); chuyifan@bgrimm.com (Y.C.); luyao@bgrimm.com (Y.L.)

² National Centre for International Research on Green Metal Mining, Beijing 102628, China

* Correspondence: likun@bgrimm.com (K.L.); guolijie@bgrimm.com (L.G.)

Abstract: The disposal of tailings has always been a focal point in the mining industry. Semi-dry tailings stockpiling, specifically high-concentration tailings stockpiling, has emerged as a potential solution. To enhance the stability of tailings stockpiling and minimize its costs, the incorporation of a low-cost curing agent into high-concentration tailings is essential. Therefore, this study focuses on the development of a curing agent for high-concentration unclassified tailings stockpiling. The composition of a low-cost curing agent system is determined based on theoretical analysis, and the curing reaction mechanisms of each composition are researched. Subsequently, an orthogonal experiment is designed, and the strength of the modified unclassified tailings solidified samples at different curing ages is measured. Furthermore, the rheological properties of the modified unclassified tailings slurries are tested, and the feasibility of industrial transportation of the unclassified tailings slurries modified with the optimized curing agent is analyzed. Lastly, the microscopic morphologies of each material and the modified unclassified tailings solidified samples are characterized, their chemical compositions are tested, and the action mechanism of the curing agent in the curing system is further investigated. The results show that the optimal proportions of each material in the curing agent are as follows: slag, 58%; quicklime, 15%; cement, 8%; gypsum, 9%; and bentonite, 10%. The dominance of industrial waste slag exceeding 50% reflects the low-cost nature of the curing agent. Under this condition, the modified unclassified tailings slurry with a mass concentration of 75% exhibited a yield stress of 43.62 Pa and a viscosity coefficient of 0.67 Pa·s, which is suitable for pipeline transportation. These findings lay a foundation for subsequent decisions regarding stockpiling processes and equipment selection.

Keywords: unclassified tailings; stockpiling; curing agent; uniaxial compressive strength; rheological characteristics



Citation: Wang, W.; Li, K.; Guo, L.; Wang, S.; Chu, Y.; Lu, Y. Curing Agent for High-Concentration Unclassified Tailings Stockpiling: A Case Study of Tailings from a Gold Mine. *Minerals* **2024**, *14*, 884. <https://doi.org/10.3390/min14090884>

Academic Editors: Yuye Tan, Xun Chen, Yuan Li and Carlito Tabelin

Received: 26 June 2024

Revised: 20 August 2024

Accepted: 26 August 2024

Published: 29 August 2024



Copyright: © 2024 by the authors. Licensee MDPI, Basel, Switzerland. This article is an open access article distributed under the terms and conditions of the Creative Commons Attribution (CC BY) license (<https://creativecommons.org/licenses/by/4.0/>).

1. Introduction

Tailings are waste materials left over from mineral processing [1]. The disposal of tailings has always been a focal point in the mining industry [2]. In recent years, incomplete statistics have indicated that China annually produces over a billion tons of tailings. As mineral resources are being extracted from deeper levels and ore grades decrease, the amount of tailings generated is increasing, making their disposal an increasingly challenging task [3]. Currently, there are three main methods for tailings disposal: wet tailings stockpiling, dry tailings stockpiling, and semi-dry tailings stockpiling, also known as high-concentration tailings stockpiling [4]. Wet tailings stockpiling involves storing tailings within a dam that contains a significant amount of water. While water is a factor in tailings dam disasters, it also plays a crucial role in exacerbating the risk of dam breaches [5,6], posing a serious threat to the safety of wet tailings stockpiling and potentially leading to pollution issues in soil, water bodies, and the atmosphere [7]. Dry tailings stockpiling requires dewatering the tailings slurry to form tailings cakes before disposal [8,9], but this method has drawbacks,

such as high costs, a low production capacity, complex procedures, and discontinuous operations. Semi-dry tailings stockpiling involves concentrating low-concentration tailings to high-concentration levels (65%–75%), and then adding a curing agent to the mixture before discharging it through pipes for stockpiling [10]. This method overcomes the disadvantages of both wet and dry tailings stockpiling and holds promising application prospects [11–13]. Currently, in this field of research, the development of low-cost curing agents is a shared goal among scholars and industry players. Furthermore, utilizing unclassified tailings for stockpiling can reduce the cost of tailings classification, simplify processes, and lower overall stockpiling expenses. Therefore, this study focuses on the development of a low-cost curing agent for high-concentration unclassified tailings from a gold mine.

Research on curing agents in the field of unclassified tailings stockpiling is limited. A comparative analysis revealed that this study can draw insights from the research on cementitious materials in the context of mine tailings backfilling. However, there are notable differences between the two. In the mine tailings backfilling domain, there is a higher demand for the curing effectiveness of cemented tailings backfill, including requirements for high strength, rapid solidification, and good integration of the tunnel roof [14–16], whereas in unclassified tailings stockpiling, the primary focus is on achieving low costs and appropriate strength. Furthermore, the proportion of curing agent to tailings (referred to as PCGT) is a crucial factor in cost control. Typically, when a certain level of solidification strength is achieved, lower PCGTs result in reduced stockpiling costs. This study explores a low-cost curing agent under the condition of a low PCGT of 1:20.

In the initial stages of mine tailings backfilling, traditional curing agents, such as ordinary Portland cement, were commonly used. However, these agents were associated with high costs and significant environmental pollution due to the substantial CO₂ emissions generated during cement production [17]. To reduce the cost of mine tailings backfilling, researchers have been actively seeking inexpensive alternatives to cement. This has led to the development of new types of cementitious materials, which essentially involve using alkalis, salts, or composite activators to stimulate potential reactive volcanic ash materials like slag and fly ash [18,19]. The goal is to transform these materials into water-hardening substances. These innovative cementitious materials include red mud-based binders [20], slag-based binders [21], and composite cementitious materials [22], among others. Analysis reveals that slag, with its relatively low cost, is chosen more extensively among these options. Slag is considered a high-activity and high-quality industrial waste resource. Its high reactivity and easy grindability make it an excellent supplementary material, which has already been widely applied in cement-based construction materials and concrete engineering. In the context of backfilling materials, slag can effectively delay the heat of hydration, increase the thickness of the water film around particles, and improve the flowability of the backfilling material. Moreover, slag possesses inherent hydration characteristics that can be activated using cement, sodium hydroxide, calcium hydroxide, sodium silicate, or gypsum [23]. Telesca et al. [24] studied and obtained prefabricated building materials composed of 40% natural or flue gas desulfurization gypsum, 35% calcium hydroxide, and 25% fly ash. Yum et al. [25] used Ca(OH)₂- and Ba(OH)₂- to activate slag systems for eco-friendly concrete brick production, and limestone fines was studied as a supplementary material in activated slags. Li et al. [26] researched the possibility of using the residues after iron recovery from iron ore tailings as raw materials for the preparation of cementitious material, which was prepared by blending a mixture of 30% residues, 34% blast-furnace slag, 30% clinker, and 6% gypsum. Yao et al. [27] found that the pozzolanic activity of iron ore tailings is improved after mechanical activation, and the hydration products of CaO-activated tailings are C-S-H gels, as well as ettringite crystals in the presence of anhydrite. Barati et al. [28] investigated the stabilization of iron ore tailings with cement and bentonite. It was found that the introduction of cement/bentonite to iron ore tailings requires higher water content for optimum compaction and results in lower dry density. The addition of bentonite greatly improves the strength of tailings–cement mixtures, especially after a period of moist curing. Fall et al. [29] studied the feasibility of using bentonite–paste

tailings as a barrier (liner, cover) material for mine waste containment facilities. Opiso et al. [30,31] found that tailings are simultaneously stabilized and can be repurposed a construction material via geopolymerization using coal fly ash, palm oil fuel ash, and a powder-based alkali activator.

Based on the factors mentioned above, we developed a curing agent to be used in high-concentration unclassified tailings stockpiling from a gold mine. The composition of this agent includes materials such as slag, quicklime, cement, gypsum, and bentonite. By analyzing the optimal proportions of each material, we aimed to create a solidified system that exhibits strong uniaxial compressive strength when solidified with the tailings. This is crucial to ensure the stability of tailings stockpiling. In addition, the rheological properties of the high-concentration unclassified tailings slurry after modification with the curing agent are vital parameters in the design of the pipeline transport and discharge processes [32–34]. These properties directly influence the sedimentation characteristics and slope of the tailings stockpiling surface [35,36], thereby affecting the safe operation and management of the tailings dam [13]. Therefore, while researching the low-cost aspects of the curing agent and ensuring it meets the strength requirements, it is also important to consider the rheological characteristics of the slurry after modification with the curing agent.

This study is based on the composition of a curing agent using the following research steps: The curing reaction mechanisms of each material in the curing agent were analyzed theoretically. Then, an orthogonal experiment was designed, the strength of the modified unclassified tailings solidified samples (MUTSSs) at different curing ages was measured, and the variation characteristics of the MUTSSs' strength and the influence of various materials at different levels on the strength were analyzed. Next, experiments were conducted to assess the rheological properties of the slurry, and the optimal proportions of each material in the curing agent were determined. Concurrently, the microscopic surface morphology of each material and MUTSSs with the optimal curing agent were characterized using scanning electron microscopy (SEM). Finally, the chemical compositions of the MUTSSs with the optimal curing agent were measured using an X-ray diffraction (XRD) test, and the action mechanism of the curing agent in the curing system was further investigated.

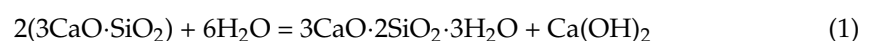
2. Curing Reaction Mechanisms

2.1. Reaction Mechanism of Cement

The primary mineral compositions of cement include tricalcium silicate (chemical formula $3\text{CaO}\cdot\text{SiO}_2$, referred to as C_3S), dicalcium silicate (chemical formula $2\text{CaO}\cdot\text{SiO}_2$, referred to as C_2S), tricalcium aluminate (chemical formula $3\text{CaO}\cdot\text{Al}_2\text{O}_3$, referred to as C_3A), and tetracalcium aluminoferrite (chemical formula $4\text{CaO}\cdot\text{Al}_2\text{O}_3\cdot\text{Fe}_2\text{O}_3$, referred to as C_4AF). The reactions of these four compositions with water are as follows [37,38]:

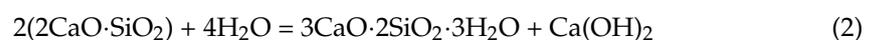
(1) Hydration of C_3S

At normal temperatures, tricalcium silicate reacts with water to form hydrated calcium silicate gel (C-S-H) and $\text{Ca}(\text{OH})_2$.



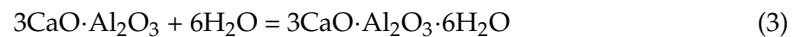
(2) Hydration of C_2S

The product of dicalcium silicate reacting with water at normal temperatures is the same as that of tricalcium silicate, but the hydration rate is slower.



(3) Hydration of C_3A

The product of tricalcium aluminate's hydration is hydrated calcium aluminate (unstable), and the reaction rate is very fast.



(4) Hydration of C₄AF

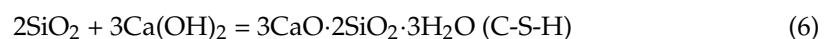
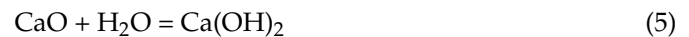
The hydration product of tetracalcium aluminoferrite includes hydrated calcium aluminate and hydrated calcium iron oxide. The reaction rate is slower than that of tricalcium aluminate.



Tricalcium aluminate and tetracalcium aluminoferrite hydrate early in the hydration process. Their hydration products combine with gypsum to form ettringite (AFt) or monosulfate hydrate (AFm), which mainly act as binding agents between particles, enhancing the fluidity of the slurry and contributing to good strength after setting. Tricalcium silicate and dicalcium silicate generally hydrate in the middle-to-later stages of the hydration process. Their hydration products mainly consist of calcium hydroxide crystals (C-H) and C-S-H gel. Calcium silicate gel is a primary source of cement strength and durability, while C-H provides an alkaline environment for hydration reactions and can continue to react with active SiO₂ to generate additional calcium silicate gel, contributing to increased strength.

2.2. Reaction Mechanism of Quicklime

Quicklime primarily consists of CaO and readily undergoes chemical reactions upon contact with water. When introduced into the fulling tailings slurry, quicklime reacts with water to generate Ca(OH)₂. Ca(OH)₂ combines with the oxides of silicon, aluminum, and small amounts of aluminum and magnesium present in the tailings and slag, forming stable hydrated calcium silicates. These hydrated silicates possess higher gel strength than Ca(OH)₂ crystals. As a result, the modified fulling tailings slurry exhibits a denser structure upon curing. The reaction equations for this entire process are depicted in Equations (5)–(7) [39,40].



2.3. Reaction Mechanism of Slag

The hydration process of slag begins with the volcanic ash reaction between active SiO₂, Al₂O₃ in the slag, and Ca(OH)₂. This reaction follows the patterns outlined in Equations (6) and (7). Continuous moisture supply in the slurry system contributes to the formation of an alkaline film on the surface of the slag. Simultaneously, the water-hydrated products infiltrate through gaps on the surface, causing further corrosion of the slag and the continuation of volcanic ash reactions until complete hydration of the slag. Additionally, gypsum present in the curing agent acts as a sulfate activator, the mechanism of which is described in Section 2.4.

2.4. Mechanism of Gypsum Hydration

The primary chemical composition of gypsum is CaSO₄, and its hydration product is calcium sulfate dihydrate [41].

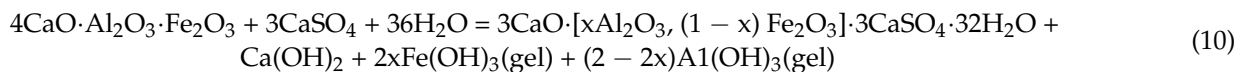


Hydrated calcium aluminate (C-A-H), formed by the reaction between active Al_2O_3 in the slag and $\text{Ca}(\text{OH})_2$, reacts with calcium sulfate dihydrate to produce calcium sulfoaluminate, commonly known as ettringite (AFt) [42].



The formation of ettringite consumes the main hydration product of hydrated calcium aluminate from slag, thus accelerating the hydration process. Simultaneously, the newly generated hydrated calcium sulfoaluminate increases the compactness of the structure itself. This product contains a high water content, significantly reducing free water, resulting in a denser structure and higher compressive strength in the solidified samples.

Moreover, the primary chemical reaction between iron phase in the slag and gypsum is as follows [43,44]:



If the amount of gypsum is relatively low, ettringite can react with tricalcium aluminate to convert it into monosulfate hydrate (AFm) [45,46].



2.5. Reaction Mechanism of Bentonite

Bentonite's main composition is montmorillonite, accounting for about 85-90%. Montmorillonite crystals primarily consist of layered aluminum silicates with water molecules. Its structure comprises two layers of silico-oxygen tetrahedra sandwiched between a layer of aluminum-oxygen octahedra, forming a 2:1 layer structure [47,48]. In the crystal structure of montmorillonite, Al^{3+} in the octahedral layer can be substituted by ions like Mg^{2+} and Fe^{3+} , while Si^{4+} in the tetrahedral layer is often partially replaced by Al^{3+} . These lattice substitutions lead to an imbalance of charges between the layers, resulting in a negatively charged interlayer of montmorillonite. To maintain charge balance, large-radius cations, such as K^+ , Na^+ , and Ca^{2+} , are adsorbed between the structural units of montmorillonite through electrostatic forces [49].

In the presence of water, the interlayer ions of montmorillonite undergo hydration, causing the montmorillonite crystals to expand. When water is added to a cementitious system, the minerals on the montmorillonite surface immediately react with water in a process known as hydrolysis or hydration. This process gradually forms hexagonal plate-like hydration products: $\text{Ca}(\text{OH})_2$, C-S-H, and AFt. This process involves a significant ion exchange, such as Ca^{2+} , Al^{3+} , Fe^{3+} , Si^{4+} , H^+ , etc., further promoting the hydration reactions in the solidification system. This exchange enhances the structural stability of the solidification system. Moreover, the expanded bentonite supports the solidification system after expansion, thereby improving the compressive strength of the system.

In conclusion, in addition to their inherent cementitious activity, the excitation agents such as cement, quicklime, and gypsum in the curing agent also serve as alkaline excitation agents for the volcanic ash reactions of slag and tailings. The synergistic effects of multiple compositions cause the active compositions in slag and tailings to dissolve and react continuously. On the one hand, the alkaline compositions provide conditions for the formation of C-S-H and C-A-H, facilitating the disintegration of the slag glass network by stimulating the release of Ca^{2+} with lower bond energies in the presence of OH^- from the slag glass body to the solution. The generated $\text{Ca}(\text{OH})_2$, along with active Al_2O_3 and SiO_2 in the slag glass network and tailings, reacts to form C-S-H and C-A-H, promoting the further disintegration of the slag glass network and the dissolution of tailings. On the other hand, gypsum reacts with active Al_2O_3 in slag and tailings to generate AFt or AFm. With the continuous generation of AFt, an amount of $\text{Ca}(\text{OH})_2$ is consumed, leading to its reduced concentration. Additionally, an amount of Al^{3+} in the solution is consumed, promoting

the dissolution of Ca^{2+} in the slag glass body and providing the driving force for ongoing chemical reactions. The mutual reinforcement of these two aspects fully stimulates the potential activity of slag. Aft/AFm and C-S-H are generated during the hydration process of slag cementitious materials, playing a crucial role in the later-stage strength and stability of the hardened body. As an additive, bentonite enhances the strength of the solidified sample through two aspects: the ion exchange among various compositions, strengthening the interactions between them, and volume expansion, reinforcing the support of the solidification system.

3. Experimental Materials and Equipment

3.1. Experimental Materials

(1) Unclassified tailings

In this study, the unclassified tailings from a gold mine in Yantai City, Shandong Province, China, were selected as a case study. The basic physical properties are described in Table 1, and the size distribution curve of the unclassified tailings particles is displayed in Figure 1. It can be observed that the cumulative content of particles with a diameter smaller than $10.0\ \mu\text{m}$ is approximately 24%, and the cumulative content of particles with a diameter smaller than $20.0\ \mu\text{m}$ exceeds 37%. The main chemical compositions in the unclassified tailings are shown in Figure 2. As shown, the content of SiO_2 is 58.3%, which is the main component, indicating that the tailings have good inertness and are suitable for stockpiling. The contents of Al_2O_3 , K_2O , and CaO are 13.35%, 5.36%, and 3.1%, respectively, which can promote the solidification of the slurry and improve the later strength of the solidified modified tailings. The content of S is 1.12%, which is relatively low and can enhance the strength of solidified modified tailings to a certain extent [50].

(2) Slag

S95-grade slag was selected, with a content of inorganic substances, like reactive calcium, silicon, and aluminum exceeding 30%, and a fineness of 325 mesh.

(3) Quicklime

Quicklime powder was chosen, with a CaO content of 86.3%, and a fineness of 325 mesh.

(4) Cement

Composite silicate cement 42.5 was selected, with the following parameters: a clinker + gypsum ratio greater than 50% and less than 80%, a physical and chemical blast furnace + volcanic ash + fly ash + limestone content ratio greater than 20% and less than 80%.

(5) Gypsum

The content of $\text{CaSO}_4 \cdot 2\text{H}_2\text{O}$ was 95%, with a fineness of 150 mesh.

(6) Bentonite

Ca-bentonite was selected, with a montmorillonite content of 85% and a fineness of 200 mesh.

Table 1. Basic physical properties of tailings.

Specific Gravity	Bulk Density (t/m)	Porosity (%)	Angle of Repose (°)
2.863	1.694	36.134	40.538

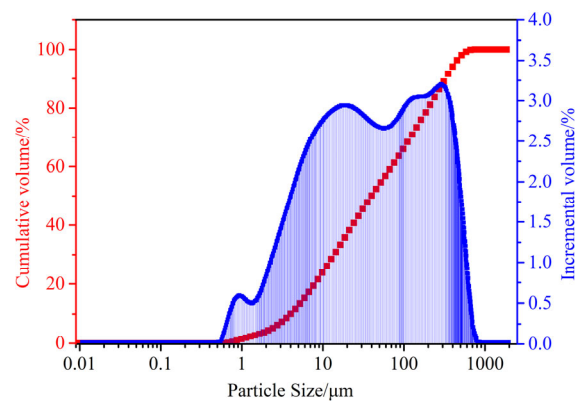


Figure 1. Unclassified tailings' particle size distribution curve.

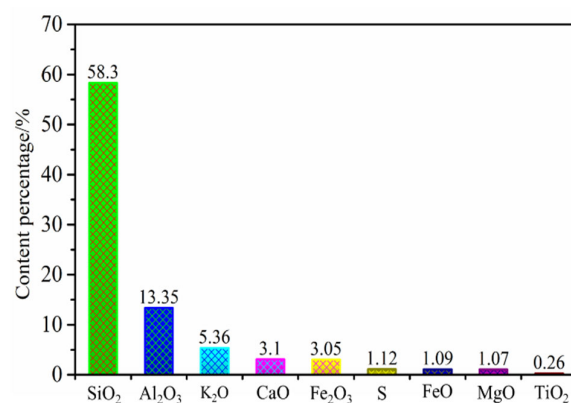


Figure 2. Unclassified tailings' chemical composition.

3.2. Experimental Equipment

(1) Load Testing Machine

An American Humboldt HM-5030 load testing machine (Humboldt Mfg. Co., Elgin, IL, USA, Figure 3a) was used. Its main technical specifications include a maximum test force of 50 kN, a maximum travel of 100 mm, and a loading rate range from 0.00001 mm/min to 89.99999 mm/min.

(2) Rheometer

An American Brookfield RST-SST Rheometer (AMETEK Brookfield, Middleboro, MA, USA, Figure 3b) was operated, with a wide torque range of 0.05–50 mNm and a variable speed range of 0.01–1000 rpm.

(3) SEM

A German Zeiss SIGMA SEM (Zeiss, Oberkochen, Germany, Figure 3c) was used, with a secondary electron image resolution of up to 1.3 nm (20 kV) and a magnification range of 20× to 1,000,000×.

(4) XRD

A Japanese X-ray diffractometer (Figure 3d), model Smartlab 9Kw (Rigaku Corporation, Tokyo, Japan), was employed. The X-ray tube focal spot size was $\leq 0.3 \times 8 \text{ mm}^2$; an all-purpose matrix detector: effective detector area $\geq 300 \text{ mm}^2$; goniometer: radius $\geq 300 \text{ mm}$; rotation range: -10° to 168° .

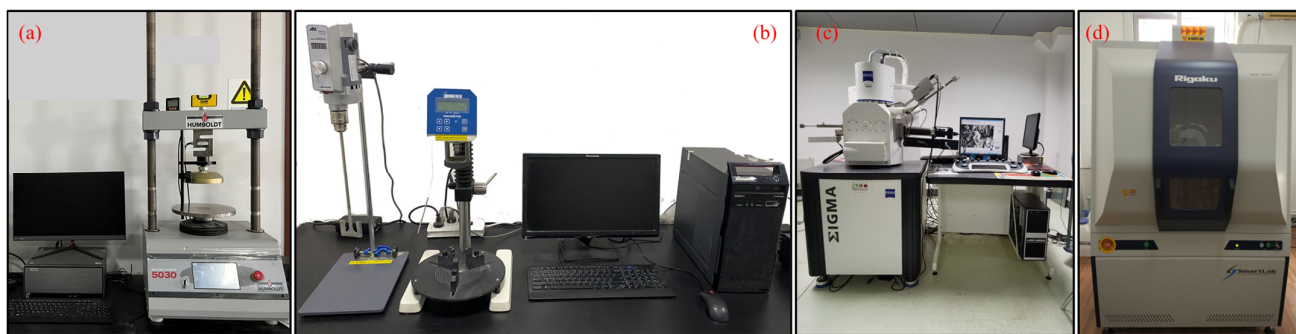


Figure 3. Experimental equipment. (a) Humboldt HM-5030 load testing machine; (b) Brookfield RST-SST Rheometer; (c) Zeiss SIGMA SEM; and (d) X-ray diffractometer.

4. Compressive Strength Testing Experiment Scheme

4.1. Orthogonal Experimental Design

During the experiment, the concentrations of the unclassified tailings slurry were set at 69%, 71%, 73%, and 75%. This study aimed to establish a solidification and stockpiling system for unclassified tailings with a relatively low PCGT. Therefore, this study focuses on the solidification effect under a PCGT of 1:20. As slag is the main composition of the curing agent and has a relatively low unit price, it is necessary to increase the proportion of slag in the curing agent to control costs, with the goal of keeping it above 50%. Therefore, when designing the proportions of the various compositions of the curing agent, this aspect should be taken into account. In addition, according to theoretical analysis, the reaction of the solidification system is faster and more complete in alkaline environments, so the proportion of quicklime should be higher. The ranges and equal divisions of the proportions of each material in the curing agent designed are shown in Table 2 [51].

Table 2. Ranges and equal divisions of proportions of each material.

	Upper Limit/%	Lower Limit/%	Equal Division/%
B (Quicklime)	30	15	5
C (Cement)	16	4	4
D (Gypsum)	12	3	3
E (Bentonite) *	10	1	3

* The remaining composition is A (slag).

Based on this, an orthogonal experiment was designed to analyze the influence of different materials on the compressive strength of the unclassified tailings solidified samples. The orthogonal experiment was designed with 5 factors and 4 levels; namely, L16(4⁵), requiring at least 16 experimental trials. The orthogonal experimental design is shown in Table 3. The laboratory sample preparation presented in Table 3 was carried out for the experiments.

Table 3. Orthogonal experimental design table.

No.	O (Unclassified Tailings Slurry Concentration) *	B (Quicklime)	C (Cement)	D (Gypsum)	E (Bentonite)	A (Slag)
1	69%	30%	16%	12%	10%	32%
2	69%	25%	12%	9%	7%	47%
3	69%	20%	8%	6%	4%	62%
4	69%	15%	4%	3%	1%	77%

Table 3. Cont.

No.	O (Unclassified Tailings Slurry Concentration) *	B (Quicklime)	C (Cement)	D (Gypsum)	E (Bentonite)	A (Slag)
5	71%	30%	12%	6%	1%	51%
6	71%	25%	16%	3%	4%	52%
7	71%	20%	4%	12%	7%	57%
8	71%	15%	8%	9%	10%	58%
9	73%	30%	8%	3%	7%	52%
10	73%	25%	4%	6%	10%	55%
11	73%	20%	16%	9%	1%	54%
12	73%	15%	12%	12%	4%	57%
13	75%	30%	4%	9%	4%	53%
14	75%	25%	8%	12%	1%	54%
15	75%	20%	12%	3%	10%	55%
16	75%	15%	16%	6%	7%	56%

* Slurry concentration = (curing agent + tailing)/(curing agent + tailing + water).

4.2. Sample Preparation

According to the number of samples and the total mass required for the experiment, combined with the information in Table 3, the mass of each material was calculated. We used the JS30-1 electronic balance (with a range of 3 kg and accuracy of 0.1 g), Shanghai Puchun Measure Instrument Co., Ltd., Shanghai, China, to measure the corresponding masses of each material. We mixed the materials in a UJZ-15 planetary mixer for 3 min (rotation speed of 120 r/min) and then poured the mixed slurry into the three-part mold (each part size was 7.07 cm × 7.07 cm × 7.07 cm). After a certain period, the samples were demolded and placed in a standard curing chamber. The temperature was set at 20 ± 5 °C and the relative humidity was above 95%. The samples were left to cure for 7 d, 14 d, and 28 d (including the time before demolding), and then their compressive strength was tested. The process is illustrated in Figure 4. In this study, we produced 192 samples.

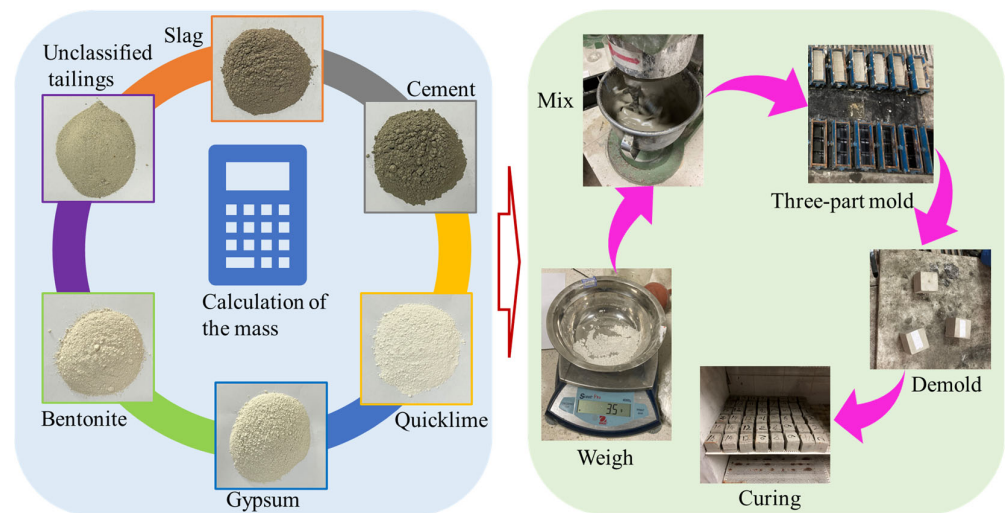


Figure 4. Schematic diagram of sample preparation process.

4.3. Compression Strength Testing

The loading rate for the test was set at 3 mm/min. The experiment was stopped when the sample was fractured and the compression displacement of the sample exceeded 18 mm. The uniaxial compression strength of the unclassified tailings solidified sample was calculated using Equation (12):

$$R_n = \frac{F}{S} \tag{12}$$

where R_n is the compression strength of the sample after n days of curing, in MPa. F is the maximum load, in N. S is the cross-sectional area of the sample perpendicular to the loading direction, in m^2 .

When calculating the average compression strength for each group of samples, the arithmetic mean was calculated using Equation (13):

$$R_{\bar{n}} = \sum_{i=1}^k \frac{R_{ni}}{k} \quad (13)$$

where $R_{\bar{n}}$ is the average compression strength after n days of curing, in MPa. R_{ni} is the experimental value of the compression strength for the i -th sample after n days of curing, in MPa. k is the number of samples in the group.

4.4. Rheological Characteristics Testing Experiment Plan

Based on the results of the uniaxial compression tests and the determined proportions of each material in the curing agent, the rheological parameters of the slurries with curing agents were tested to analyze the flow properties of each slurry and determine the optimal proportions of each material in the curing agent. During the experiment, the corresponding weights of the unclassified tailings, curing agent, and water were weighed. The modified unclassified tailings slurries were prepared following the procedure outlined in Section 4.2. Once the slurry was uniformly mixed, it was poured into a 500 mL beaker until the liquid level reached the 500 mL mark. The beaker was then placed on the rheometer sample stage and securely fixed. The height of the rotor was adjusted, and the test was initiated. As temperature can influence the viscosity coefficient of the slurry, the experiment maintained a controlled temperature of 20 ± 2 °C.

5. Results

5.1. Compression Strength Test Results

The average uniaxial compression strength values of the samples after curing periods of 7 d, 14 d, and 28 d are summarized in Figure 5. As can be seen, at the ages of 7 d, 14 d, and 28 d, the strength of samples from No. 1 to No. 16 shows a trend of fluctuation and increase. The strength values of the same samples after 7 d are less than those after 14 d, which are, in turn, less than those after 28 d. This indicates that, within 28 d, the greater the age, the more complete the reaction of the solidified material, the better the cementation effect, and the stronger the sample strength [26]. It was also found that the greater the age, the greater the range of the sample's strength and the more obvious the difference, reflecting the different reaction degrees of the same compositions in different periods.

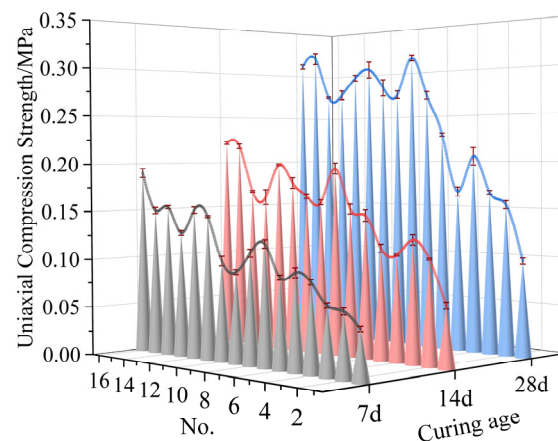


Figure 5. Average uniaxial compression strength of samples at different curing ages.

In order to intuitively show the influence of various factors at different levels on the compressive strength, the average uniaxial compressive strength values of the samples for each factor at each level were plotted, as shown in Figure 6, where k represents the average uniaxial compressive strength for each factor at each level. It can be seen that, with the changes at each level of factors O and B, the strength of the samples at 7 d, 14 d, and 28 d gradually increased, and the influence was obvious. The influence of each level of factors C, D, and E on the strength was inconsistent and not obvious.

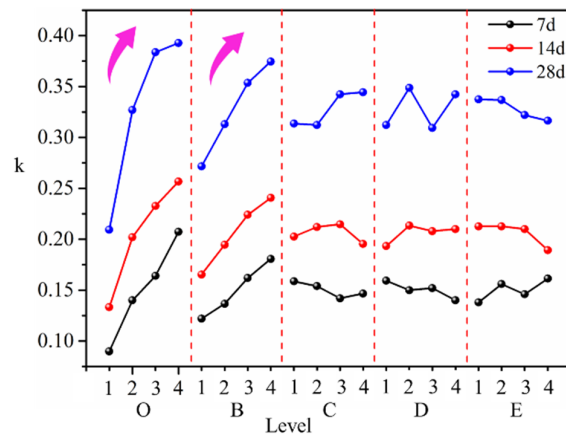


Figure 6. Influence of various factors at different levels on compressive strength.

Table 4 shows the range analysis results of the orthogonal experiments, which were found according to the data in Table 3 and Figure 5. It can be observed that the influence of various factors on the compressive strength of the samples at 7 d and 14 d follows the order of $O > B > E > D > C$, and the influence of various factors on the compressive strength of samples at 28 d follows the order of $O > B > D > C > E$, indicating that the compressive strength was primarily affected by the slurry concentration and the proportion of quicklime. Based on the test results, the optimal combination proportions of the materials in the curing agent at different curing ages are shown in Table 5.

Table 4. Results of range analysis of orthogonal experiments.

	Curing Age	O	B	C	D	E
Range R	7 d	0.117	0.059	0.017	0.019	0.023
	14 d	0.123	0.075	0.019	0.020	0.023
	28 d	0.183	0.103	0.032	0.039	0.021
Main-Sub Sequence	7 d	$O > B > E > D > C$				
	14 d	$O > B > E > D > C$				
	28 d	$O > B > D > C > E$				
Optimal Level	7 d	O4	B4	C1	D1	E4
	14 d	O4	B4	C3	D2	E1
	28 d	O4	B4	C4	D2	E1

Table 5. Optimal mass proportions of various materials at different curing ages.

Curing Age	Slurry Mass Concentration	Mass Proportion				
		Slag	Quicklime	Cement	Gypsum	Bentonite
7d	75%	56%	15%	16%	12%	1%
14d	75%	58%	15%	8%	9%	10%
28d	75%	62%	15%	4%	9%	10%

5.2. Rheological Characteristics Test Results

The rheological parameters of the modified tailings slurries were tested based on the three curing agent proportions above. In this study, the curing agent proportions corresponding to the best flowability were identified as the optimal proportions. The rheological characteristics of the three modified tailings slurries are illustrated in Figure 7. As shown, the regression curves of the flow curves for the modified tailings slurries I (7 d), II (14 d), and III (28 d) were represented by blue, green, and orange dashed lines, respectively. The regression equations for the flow curves of the modified tailings slurries I (7 d), II (14 d), and III (28 d) were, respectively, $\tau_I = 26.07 + 0.89\gamma$, $\tau_{II} = 43.62 + 0.67\gamma$, and $\tau_{III} = 30.59 + 0.71\gamma$, and all R^2 values were greater than 0.90, indicating that all three modified tailings slurries adhered to the Bingham fluid model. The yield stresses of the slurries were 26.07 Pa, 43.62 Pa, and 30.59 Pa, and the viscosity coefficients of the slurries were 0.89 Pa·s, 0.67 Pa·s, and 0.71 Pa·s, respectively.

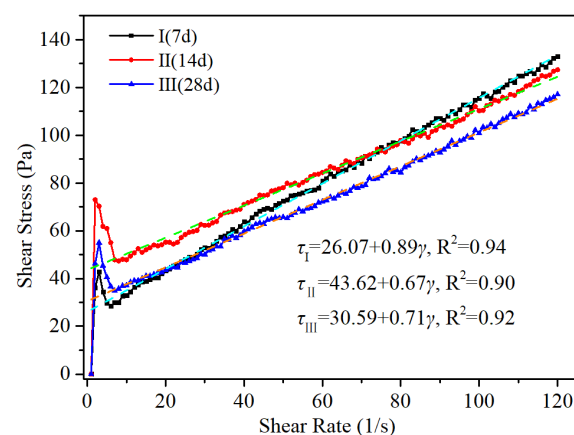


Figure 7. Rheological curves of the three modified tailings slurries.

Grabinsky et al. believed that the yield stress of high-concentration tailings is generally greater than 20 Pa but less than 100 Pa, and high-concentration tailings can be efficiently transported using centrifugal pumps [52]. Despite being high-concentration tailings, they still retain some paste-like characteristics. Their rheological behavior falls within the non-Newtonian realm, yet their yield stress is noticeably lower than that of conventional pastes. This property results in lower pipeline transportation resistance and reduced self-flowing gradients. The outcome in this study is consistent with the findings of Grabinsky et al. The yield stress indicates the threshold at which flow starts in response to shear stress exceeding the yield stress. This is typical of Bingham fluids, which only begin to flow when the applied shear stress surpasses the yield stress. The viscosity coefficient represents internal resistance to flow, and the smaller the value, the better the slurry flow [53]. Therefore, the optimal condition occurs when the yield stress is 43.62 Pa and the viscosity coefficient is 0.67 Pa·s. This corresponds to a tailings slurry concentration of 75%, with the curing agent consisting of slag (58%), quicklime (15%), cement (8%), gypsum (9%), and bentonite (10%).

Gao et al. researched the fluid characteristics of the cemented backfill pipeline transportation of mineral processing tailings [54]. It was concluded that the viscosity coefficient of the slurry concentration reached 24.42607 Pa·s at 80% and 3.73863 Pa·s at 78%. When the concentration was 76%, the viscosity coefficient decreased to 1.21629 Pa·s, and at 74% and 72%, it decreased to 0.58072 Pa·s and 0.31388 Pa·s, respectively. If the viscosity coefficient is too large, it results in excessive resistance during the transportation of slurry when only a high-pressure piston pump is feasible. Thus, the yield stress of 43.62 Pa and the viscosity coefficient of 0.67 Pa·s obtained in this study renders the slurry suitable for pipeline transportation [34,36], laying a foundation for subsequent decisions regarding stockpiling processes and equipment selection.

5.3. SEM Experimental Results

As shown in Figure 8a, slag particles primarily exhibit cubic, blocky, and irregular shapes, with distinct edges and a dense texture. The particle sizes range from approximately 1 to 10 μm . Nanoscale particles are attached to the surface of larger particles, which appear relatively smooth. Figure 8b reveals that the particles of quicklime are mainly clustered, forming uniform-sized crystal branches. The size of each branch is smaller than 1 μm , and they aggregate to form structures ranging from 1 to 10 μm , characterized by a rough surface with occasional protrusions. The aggregated structures formed by the branches appear loose and porous. Figure 8c illustrates that cement particles exist in various forms, including blocks, rods, spheres, cubes, and irregular shapes, displaying substantial shape variation. Nanoscale particles are attached to the surfaces of larger particles (size > 2 μm), leading to rough surfaces on the larger particles. Rod-like particles have dimensions of approximately 2 $\mu\text{m} \times 10 \mu\text{m}$, and their surface roughness lies between that of the larger and spherical particles. In Figure 8d, gypsum is primarily present in flocculent, small-particle, large-block, and irregular forms. Flocculent small particles exhibit multiple protrusions and a rough surface. Figure 8e shows that most bentonite particles exhibit circular, elliptical, or similar circular shapes, with rough surfaces and sizes ranging from a few micrometers to tens of micrometers. Figure 8f demonstrates the varied sizes of the unclassified tailings particles, with the largest particle in the image measuring about 200 $\mu\text{m} \times 300 \mu\text{m}$. The majority of particles have sizes below a few micrometers, some even in the nanometer range. In addition, most of the tailings appear as flakes, and it can be seen that the surface of the tailings is rough.

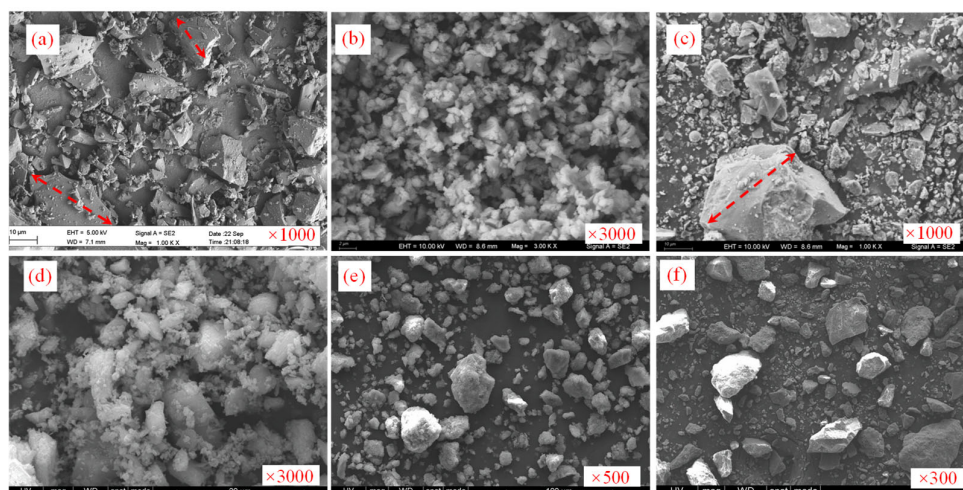


Figure 8. Microscopic morphology of various materials: (a) slag, (b) quicklime, (c) cement, (d) gypsum, (e) bentonite, and (f) unclassified tailings.

Figure 9 illustrates the cross-sectional morphology of the modified tailings solidified samples with the optimal curing agent. It can be observed that after the reaction, the various materials were fused together as a whole, and the sharp edges of the material particles disappeared. Additionally, the disappearance of the quicklime morphology indicates that the quicklime underwent a full reaction. The surfaces of some tailings particles were involved in the hydration reaction, and the rest is wrapped by the hydration products. The tailings particles that were not fully reacted, as shown by the brown arrow, acted as a skeleton, and supported the strength of the solidified samples. The hydration products were mainly AFt (prismatic ettringite) and C-S-H [51,55]. The appearance of a flocculent gel system can be observed; some gel systems exhibited clear spatial structures, as indicated by the red dashed line. The green arrows indicate the pore structure. These characteristics enhanced the strength of the solidified sample. Comprehensive analysis revealed that effective reactions occurred between the curing agent and the unclassified tailings, resulting

in gel systems and spatial structures, thereby enhancing the overall strength of the solidified system and achieving effective solidification of the unclassified tailings.

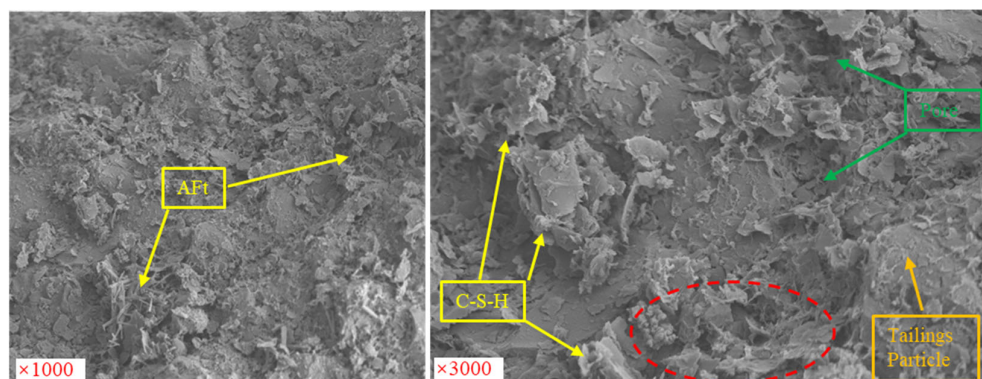


Figure 9. Microscopic morphology of a modified unclassified tailings solidified sample. (AFt mainly presented as needle shaped, columnar, prismatic, etc. C-S-H mainly presented as cotton-like, network-like, and floc-like structures).

6. Discussion

Further experimentation revealed that the average uniaxial compression strength values of the modified unclassified tailings solidified samples with the optimal curing agent were 0.20 MPa, 0.25 MPa, and 0.34 MPa at 7 d, 14 d, and 28 d, respectively. We conducted XRD tests on these MUTSSs at different curing ages to further analyze the chemical reaction mechanism of each material in the curing agent. Figure 10 shows the XRD patterns of the MUTSSs at 7 d, 14 d, and 28 d. The diffraction peaks corresponding to C-S-H, AFt, Ca (OH)₂, CaCO₃, and SiO₂ can be seen in the figure [51,55]. Figure 11 illustrates the qualitative relationships among the main hydration products. As shown, with the extension of the hydration time, the contents of AFt and Ca (OH)₂ decreased, while the content of C-S-H increased. This phenomenon is consistent with the conclusions reported by Jha et al. [56], Telesca et al. [24], Yum et al. [25], and Li et al. [26].

When the curing time was 7 days, the AFt content was the highest, followed by C-S-H and Ca(OH)₂. At the initial stage of hydration, more AFt crystals formed, and C-S-H gel grew on the cement particles. Due to the growth of C-S-H and the formation of AFt crystals, strong and weak contact points were generated. At the same time, the hydration product particles connected to form a network, giving the solidified samples early strength. As the number of contact points increased, the size of the network structure increased, and consequently, the strength of the solidified samples increased. The combination of the hydration products, tailings, and unhydrated clinker is the reason for the observed early macroscopic strength. After 28 d of curing, the content of C-S-H was the highest, followed by AFt and Ca(OH)₂. At this time, the strength of the solidified samples was the highest. This observation can be explained as follows: After 28d of hydration, a significant amount of C-S-H was generated, enhancing the long-term strength and durability of the solidified samples. Due to the abundant presence of C-S-H and the complete formation of AFt and Ca(OH)₂ crystals, hydration products filled the space previously occupied by water. The spatial distribution of the hydration products was uniform and gradually interwoven, ultimately forming a dense multi-layered network structure, which increased the overall compressive strength. The above phenomena and analysis are consistent with the research presented in Section 2, and are a supplement to the theoretical analysis in Section 2, reflecting the phased nature of the curing reaction process.

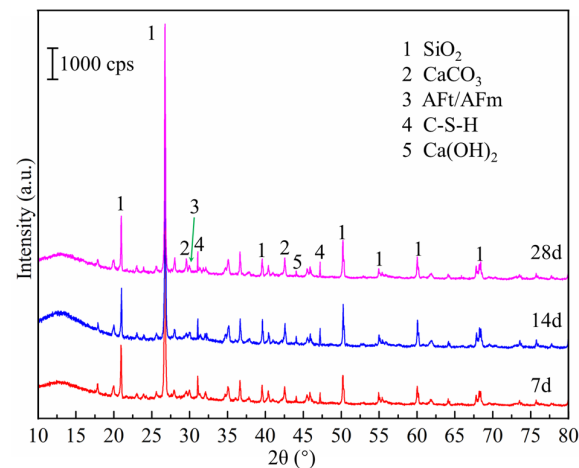


Figure 10. XRD patterns of MUTSSs.

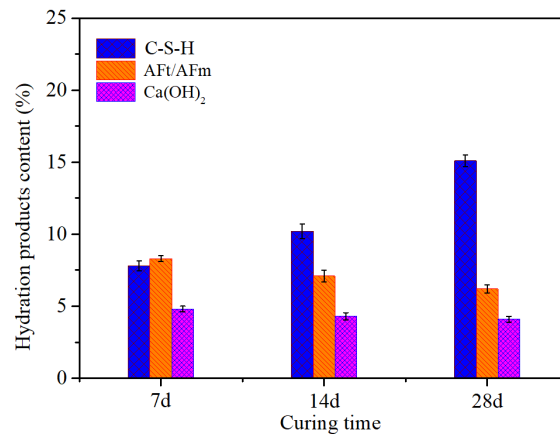


Figure 11. Qualitative relationships among the main hydration products of MUTSSs.

7. Conclusions

In this research, we conducted a theoretical analysis of chemical reactions; designed a laboratory orthogonal experiment; carried out compressive strength testing, rheological properties testing, SEM experiments, XRD experiments, etc.; and obtained low-cost curing agents suitable for high-concentration tailings stockpiling. The main conclusions are as follows:

- (1) The curing agent system for tailings consolidation and stockpiling composed of slag, quicklime, cement, gypsum, and bentonite is feasible. The reaction mechanism involves synergistic interactions among these compositions, promoting the dissolution of active compositions in slag and tailings. In addition to their inherent cementitious activity, the excitation agents such as cement, quicklime, and gypsum in the curing agent also serve as alkaline excitation agents for the volcanic ash reactions of slag and tailings. The formation of calcium hydroxide and various C-S-H/C-A-H enhances the disintegration of the slag glass network. The presence of gypsum aids in the formation of AFt or AFm through reactions with active compositions. Bentonite contributes to ion exchange and volumetric expansion, reinforcing the solidifying system;
- (2) The optimal proportions of each material in the curing agent are as follows: slag, 58%; quicklime, 15%; cement, 8%; gypsum, 9%; and bentonite, 10%. The proportion of industrial waste steel slag reached 58%, which reflects the low-cost nature of the curing agent. Under this condition, the modified unclassified tailings slurry exhibited a yield stress of 43.62 Pa and a viscosity coefficient of 0.67 Pa·s at a slurry concentration of 75%, and the average uniaxial compression strength values of the MUTSSs were 0.20 MPa, 0.25 MPa, and 0.34 MPa at 7 d, 14 d, and 28 d, respectively;

- (3) The hydration products of the curing agent are mainly Aft, C-S-H and Ca (OH)₂. With the extension of the hydration time, the contents of Aft and Ca (OH)₂ decreased, while the content of C-S-H increased, forming a gel system and spatial structures. The tailings particles that did not fully react acted as a skeleton and supported the strength of the solidified samples. These two aspects worked together to improve the overall strength of the solidified sample and achieved effective solidification of the unclassified tailings.

Author Contributions: Conceptualization, W.W., K.L. and L.G.; methodology, W.W. and K.L.; validation, K.L. and L.G.; formal analysis, Y.L. and Y.C.; investigation, S.W. and Y.C.; data curation, Y.L. and Y.C.; writing—original draft preparation, W.W. and S.W.; writing—review and editing, L.G.; supervision, L.G.; funding acquisition, K.L. and L.G. All authors have read and agreed to the published version of the manuscript.

Funding: This research received no external funding.

Data Availability Statement: The data supporting the conclusions of this article will be made available by the authors on request.

Acknowledgments: This work was supported by the National Key R&D Program of China (2022YFC2903905, 2021YFC2900600, 2021YFE0102900).

Conflicts of Interest: Weixiang Wang, Kun Li, Lijie Guo, Sha Wang, Yifan Chu and Yao Lu are employees of BGRIMM Technology Group. The paper reflects the views of the scientists and not the company.

References

1. Tabelin, C.B.; Park, I.; Phengsaart, T.; Jeon, S.; Villacorte-Tabelin, M.; Alonzo, D.; Yoo, K.; Ito, M.; Hiroyoshi, N. Copper and critical metals production from porphyry ores and E-wastes: A review of resource availability, processing/recycling challenges, socio-environmental aspects, and sustainability issues. *Resour. Conserv. Recycl.* **2021**, *170*, 105610. [\[CrossRef\]](#)
2. Liu, L.; Xin, J.; Huan, C.; Zhao, Y.J.; Fan, X.; Guo, L.J.; Song, K.-I. Effect of curing time on the mesoscopic parameters of cemented paste backfill simulated using the particle flow code technique. *Int. J. Miner. Metall. Mater.* **2021**, *28*, 590–602. [\[CrossRef\]](#)
3. Edraki, M.; Baumgartl, T.; Manlapig, E.; Bradshaw, D.; Franks, D.M.; Moran, C.J. Designing mine tailings for better environmental, social and economic outcomes: A review of alternative approaches. *J. Clean. Prod.* **2014**, *84*, 411–420. [\[CrossRef\]](#)
4. Boger, D.V. Personal perspective on paste and thickened tailings: A decade on. *Min. Technol.* **2012**, *121*, 29–36. [\[CrossRef\]](#)
5. Psarropoulos, P.N.; Tsompanakis, Y. Stability of tailings dams under static and seismic loading. *Can. Geotech. J.* **2008**, *45*, 663–675. [\[CrossRef\]](#)
6. Birch, W.J.; Dixon-Hardy, D.W.; Engels, J.M. Tailings management facility topography modelling to identify flow accumulations and pond geometry. *Min. Technol.* **2006**, *115*, 65–74. [\[CrossRef\]](#)
7. Cross, A.T.; Lambers, H. Young calcareous soil chronosequences as a model for ecological restoration on alkaline mine tailings. *Sci. Total Environ.* **2017**, *607*, 168–175. [\[CrossRef\]](#)
8. Schoenbrunn, F.; Bach, M. The Development of paste thickening and its application to the minerals industry; an industry review. *BHM Berg-Und Hüttenmännische Monatshefte* **2015**, *160*, 257–263. [\[CrossRef\]](#)
9. Newman, L.; Arnold, K.; Wittwer, D. Dry stack tailings design for the Rosemont Copper project. In *Tailings and Mine Waste*; CRC Press: Boca Raton, FL, USA, 2010; pp. 315–326. [\[CrossRef\]](#)
10. Alshawmar, F.; Fall, M. Dynamic response of thickened tailings in shaking table testing. *Int. J. Geo-Eng.* **2021**, *12*, 28. [\[CrossRef\]](#)
11. Wang, Z.W.; Li, F.; Mei, G.D. OpenMP Parallel Finite-Discrete Element Method for Modeling Excavation Support with Rockbolt and Grouting. *Rock Mech. Rock Eng.* **2024**, *57*, 3635–3657. [\[CrossRef\]](#)
12. Fourie, A. Paste and thickened tailings: Has the promise been fulfilled. In *GeoCongress 2012: State of the Art and Practice in Geotechnical Engineering*; American Society of Civil Engineers: Reston, VA, USA, 2012; pp. 4126–4135.
13. Eng, F.P.P. Paste Thickening: Considerations for Backfill vs. Tailings Management. *Eng. Min. J.* **2011**, *212*, 34–40.
14. Yang, P.Y.; Li, L. Investigation of the short-term stress distribution in stopes and drifts backfilled with cemented paste backfill. *Int. J. Min. Sci. Technol.* **2015**, *25*, 721–728.
15. Kouame, K.J.A.; Feng, Y.; Jiang, F.; Zhu, S. A Study of Technical Measures for Increasing the Roof-Contacted Ratio in Stope and Cavity Filling. *J. Mater. Sci. Res.* **2016**, *5*, 54. [\[CrossRef\]](#)
16. Chen, O.S.; Zhang, O.L.; Fourie, A.; Chen, X.; Qi, C.C. Experimental investigation on the strength characteristics of cement paste backfill in a similar stope model and its mechanism. *Constr. Build. Mater.* **2017**, *154*, 34–43. [\[CrossRef\]](#)
17. Luo, L.; Zhang, Y.; Bao, S.; Chen, T. Utilization of Iron Ore Tailings as Raw Material for Portland Cement Clinker Production. *Adv. Mater. Sci. Eng.* **2016**, *2016*, 1596047. [\[CrossRef\]](#)

18. Shi, X.; Wang, X.; Wang, X. Dual waste utilization in cemented paste backfill using steel slag and mine tailings and the heavy metals immobilization effects. *Powder Technol.* **2022**, *403*, 117413. [[CrossRef](#)]
19. Wang, J.; Fu, J.; Song, W.; Zhang, Y. Effect of rice husk ash (RHA) dosage on pore structural and mechanical properties of cemented paste backfill. *J. Mater. Res. Technol.* **2022**, *17*, 840–851. [[CrossRef](#)]
20. Chen, S.J.; Du, Z.W.; Zhang, Z.; Yin, D.W.; Feng, F.; Ma, J.B. Effects of red mud additions on gangue-cemented paste backfill properties. *Powder Technol.* **2020**, *367*, 833–840. [[CrossRef](#)]
21. Zhao, Y.L.; Ma, Z.Y.; Qiu, J.P.; Sun, X.G.; Gu, X.W. Experimental study on the utilization of steel slag for cemented ultra-fine tailings backfill. *Powder Technol.* **2020**, *375*, 284–291.
22. Zhao, Y.L.; Wu, P.Q.; Qiu, J.P.; Guo, Z.B.; Tian, Y.S.; Sun, X.G.; Gu, X.W. Recycling hazardous steel slag after thermal treatment to produce a binder for cemented paste backfill. *Powder Technol.* **2022**, *395*, 652–662. [[CrossRef](#)]
23. Zhao, Y.L.; Qiu, J.P.; Zhang, S.Y.; Guo, Z.B.; Wu, P.Q.; Sun, X.G.; Gu, X.W. Low carbon binder modified by calcined quarry dust for cemented paste backfill and the associated environmental assessments. *J. Environ. Manag.* **2021**, *300*, 113760. [[CrossRef](#)] [[PubMed](#)]
24. Telesca, A.; Marroccoli, M.; Calabrese, D.; Valenti, G.L.; Montagnaro, F. Flue gas desulfurization gypsum and coal fly ash as basic components of prefabricated building materials. *Waste Manag.* **2013**, *33*, 628–633. [[CrossRef](#)] [[PubMed](#)]
25. Yum, W.S.; Jeong, Y.; Song, H.; Oh, J.E. Recycling of limestone fines using Ca(OH)₂ and Ba(OH)₂ activated slag systems for eco-friendly concrete brick production. *Constr. Build. Mater.* **2018**, *185*, 275–284. [[CrossRef](#)]
26. Li, C.; Sun, H.H.; Bai, J.; Li, L.T. Innovative methodology for comprehensive utilization of iron ore tailings: Part I. The recovery of iron from iron ore tailings using magnetic separation after magnetizing roasting. *J. Hazard. Mater.* **2010**, *174*, 71–77. [[CrossRef](#)]
27. Yao, G.; Wang, Q.; Su, Y.W.; Wang, J.X.; Qiu, J.; Lyu, X.J. Mechanical activation as an innovative approach for the preparation of pozzolan from iron ore tailings. *Miner. Eng.* **2020**, *145*, 106068. [[CrossRef](#)]
28. Barati, S.; Tabatabaie Shourijeh, P.; Samani, N.; Asadi, S. Stabilization of iron ore tailings with cement and bentonite: A case study on Golgohar mine. *Bull. Eng. Geol. Environ.* **2020**, *79*, 4151–4166. [[CrossRef](#)]
29. Fall, M.; Célestin, J.C.; Han, F.S. Suitability of bentonite-paste tailings mixtures as engineering barrier material for mine waste containment facilities. *Miner. Eng.* **2009**, *22*, 840–848. [[CrossRef](#)]
30. Opiso, E.M.; Tabelin, C.B.; Maestre, C.V.; Aseniero, J.P.J.; Arima, T.; Villacorte-Tabelin, M. Utilization of Palm Oil Fuel Ash (POFA) as an Admixture for the Synthesis of a Gold Mine Tailings-Based Geopolymer Composite. *Minerals* **2023**, *13*, 232. [[CrossRef](#)]
31. Opiso, E.M.; Tabelin, C.B.; Maestre, C.V.; Aseniero, J.P.J.; Park, I.; Villacorte-Tabelin, M. Synthesis and characterization of coal fly ash and palm oil fuel ash modified artisanal and small-scale gold mine (ASGM) tailings based geopolymer using sugar mill lime sludge as Ca-based activator. *Heliyon* **2021**, *7*, e06654. [[CrossRef](#)]
32. Wang, Y.; Wu, A.X.; Zhang, L.F.; Wang, H.J.; Jin, F. Investigation of the Sedimentation Property of Backfill Material on the Basis of Rheological Test: A Case Study of Iron Tailings. *J. Chem.* **2018**, *2018*, 9530767. [[CrossRef](#)]
33. Boger, D.V. Rheology of slurries and environmental impacts in the mining industry. *Annu. Rev. Chem. Biomol.* **2013**, *4*, 239–257. [[CrossRef](#)]
34. Yang, L.; Jia, H.; Wu, A.; Jiao, H.; Chen, X.; Kou, Y.; Dong, M. Particle Aggregation and Breakage Kinetics in Cemented Paste Backfill. *Int. J. Miner. Metall. Mater.* **2023**, *220*, 172–186. [[CrossRef](#)]
35. Mizani, S.; He, X.; Simms, P. Application of lubrication theory to modeling stack geometry of high density mine tailings. *J. Non-Newton. Fluid Mech.* **2013**, *198*, 59–70. [[CrossRef](#)]
36. Yang, L.; Gao, Y.; Chen, H.; Jiao, H.; Dong, M.; Bier, T.A.; Kim, M. Three-dimensional concrete printing technology from a rheology perspective: A review. *Adv. Cem. Res.* **2024**, *126*, 72–86. [[CrossRef](#)]
37. Li, G.Y.; Zhao, X.H. Properties of concrete incorporating fly ash and ground granulated blast-furnace slag. *Cem. Concr. Comp.* **2003**, *25*, 293–299. [[CrossRef](#)]
38. Double, D.D. New developments in understanding the chemistry of cement hydration. *Phil. Trans. R. Soc. Lond. A* **1983**, *310*, 53–66.
39. Wang, B.W.; Li, Q.L.; Dong, P.B.; Gan, S.; Yang, L.; Wang, R.Z. Performance investigation of blast furnace slag based cemented paste backfill under low temperature and low atmospheric pressure. *Constr. Build. Mater.* **2023**, *363*, 129744. [[CrossRef](#)]
40. Zhang, M.G.; Li, K.Q.; Ni, W.; Zhang, S.Q.; Liu, Z.Y.; Wang, K.; Wei, X.L.; Yu, Y. Preparation of mine backfilling from steel slag-based non-clinker combined with ultra-fine tailing. *Constr. Build. Mater.* **2022**, *320*, 126248. [[CrossRef](#)]
41. Hou, Y.Q.; Yang, K.; Yin, S.H.; Yu, X.; Wang, L.M.; Yang, X.B. Enhancing the physical properties of cemented ultrafine tailings backfill (CUTB) with fiber and rice husk ash: Performance, mechanisms, and optimization. *J. Mater. Res. Technol.* **2024**, *29*, 4418–4432. [[CrossRef](#)]
42. Salami, B.A.; Ibrahim, M.; Algaifi, H.A.; Alimi, W.; Oladapo, E.A. A review on the durability performance of alkali-activated binders subjected to chloride-bearing environment. *Constr. Build. Mater.* **2022**, *317*, 125947. [[CrossRef](#)]
43. Yuan, H.; Chen, S.Y. Effects of titanium gypsum on high calcium fly ash system: Physical and microscopic properties, hydration, and Fe transformation. *J. Build. Eng.* **2023**, *78*, 107653. [[CrossRef](#)]
44. Xia, Y.; Liu, M.H.; Zhao, Y.D.; Chi, X.F.; Guo, J.Z.; Du, D.H.; Du, J.X. Hydration mechanism and phase assemblage of blended cement with iron-rich sewage sludge ash. *J. Build. Eng.* **2023**, *63*, 105579. [[CrossRef](#)]
45. Liu, X.H.; Ma, B.G.; Tan, H.B.; Gu, B.Q.; Zhang, T.; Chen, P.; Li, H.N.; Mei, J.P. Effect of aluminum sulfate on the hydration of Portland cement, tricalcium silicate and tricalcium aluminate. *Constr. Build. Mater.* **2020**, *232*, 117179. [[CrossRef](#)]

46. Li, C.B.; Ma, B.G.; Tan, H.B.; Zhang, T.; Liu, X.H.; Chen, P. Effect of triisopropanolamine on chloride binding of cement paste with ground-granulated blast furnace slag. *Constr. Build. Mater.* **2020**, *256*, 119494. [[CrossRef](#)]
47. Soliman, M.A.; Rashad, G.M.; Mahmoud, M.R. Organo-modification of montmorillonite for enhancing the adsorption efficiency of cobalt radionuclides from aqueous solutions. *Environ. Sci. Pollut. Res.* **2019**, *26*, 10398–10413. [[CrossRef](#)]
48. Kazutoshi, H.; Li, H.J.; MatSuda, K.; Takehisa, T.; Elliott, E. Mechanism of forming organic/inorganic network structures during in-situ free-radical polymerization in PNIPA-Clay nanocomposite hydrogels. *Macromolecules* **2005**, *38*, 3482.
49. Segad, M.; Jonsson, B.; Akesson, T.; Cabane, B. Ca/Na Montmorillonite: Structure, Forces and Swelling Properties. *Langmuir* **2010**, *26*, 5782–5790. [[CrossRef](#)]
50. Liu, L.; Xin, J.; Huan, C.; Qi, C.C.; Zhou, W.W.; Song, K.-I. Pore and strength characteristics of cemented paste backfill using sulphide tailings: Effect of sulphur content. *Constr. Build. Mater.* **2020**, *237*, 117452. [[CrossRef](#)]
51. Zhao, X.Y.; Yang, K.; He, X.; Wei, Z.; Zhang, J.Q. Study on proportioning experiment and performance of solid waste for underground backfilling. *Mater. Today Commun.* **2022**, *32*, 103863. [[CrossRef](#)]
52. Grabinsky, M.W.; Theriault, J.; Welch, D. An overview of paste and thickened tailings disposal on surface. In *Symposium 2002 on Environment and Mine*; Canadian Institute of Mining, Metallurgy and Petroleum: Montreal, QC, Canada, 2002; p. 533.
53. Leong, Y.K. Controlling the rheology of iron ore slurries and tailings with surface chemistry for enhanced beneficiation performance and output, reduced pumping cost and safer tailings storage in dam. *Miner. Eng.* **2021**, *166*, 106874. [[CrossRef](#)]
54. Gao, R.G.; Zhou, K.P.; Zhou, Y.L.; Yang, C. Research on the fluid characteristics of cemented backfill pipeline transportation of mineral processing tailings. *Alex Eng. J.* **2020**, *59*, 4409–4426. [[CrossRef](#)]
55. Gu, X.W.; Yang, B.H.; Li, Z.J.; Liu, B.N.; Liu, J.P.; Wang, Q.; Nehdif, M.L. Elucidating the reaction of seashell powder within fly ash cement: A focus on hydration products. *Constr. Build. Mater.* **2024**, *428*, 136331. [[CrossRef](#)]
56. Jha, A.K.; Sivapullaiah, P.V. Volume change behavior of lime treated gypseous soil—Influence of mineralogy and microstructure. *Appl. Clay Sci.* **2016**, *119*, 202–212. [[CrossRef](#)]

Disclaimer/Publisher’s Note: The statements, opinions and data contained in all publications are solely those of the individual author(s) and contributor(s) and not of MDPI and/or the editor(s). MDPI and/or the editor(s) disclaim responsibility for any injury to people or property resulting from any ideas, methods, instructions or products referred to in the content.